Hypercoordinated XH_{n+1} Radicals for First- and Second-Row Atoms. A Valence Bond Analysis

A. Demolliens,[†] O. Eisenstein,[†] P. C. Hiberty,*[,†] J. M. Lefour,[†] G. Ohanessian,[†] S. S. Shaik,*[,‡] and F. Volatron*[,†]

Contribution from the Laboratoire de Chimie Théorique (UA 506), ICMO, Université de Paris-Sud (Bâtiment 490), 91405 Orsay Cedex, France, and Department of Chemistry, Ben Gurion University, Beer-Sheva 84120, Israel. *Received August 31, 1987*

Abstract: A theory of hypercoordination is developed using the valence bond (VB) curve-crossing diagram model and applied to XH_{n+1} radicals that are generated by hydrogen atom attachment to a normal-valent XH_n molecule. Hypercoordinated XH_{n+1} radicals fall into two broad classes of valence species: those that can be described by a correlation and avoided crossing of their two Lewis curves, e.g., SiH_5, and those that require at least one additional curve—termed the intermediate curve—such as PH_4. The Lewis curves correspond to the electron-pairing schemes of the normal-valent constituents in the exchange process $H^{\bullet} + XH_n \rightarrow [XH_{n+1}] \rightarrow H_nX + H^{\bullet}$. The intermediate curve possesses an $(n \rightarrow \sigma^*)$ excited character and mixes into the Lewis curves, mainly at the hypercoordinated region. This mixing endows XH_{n+1} with additional stability and a new electronic character (Figure 2, **18**, **19**). A third class of XH_{n+1} radicals exists, in which the two Lewis curves are crossed by an intermediate Rydberg curve (n → R excitation) which provides an energy well to house a Rydberg XH_{n+1} radical (Figure 4). The hypercoordination capability of an atom X depends on the X–H bond of the normal-valent XH_n and on the presence of a lone pair on X. *The weaker the X–H bond, the more stable the XH_{n+1} species relative to its normal-valent constituents $XH_n + H^{\bullet}$. The XH_{n+1} species gains additional stability that is proportional to the ease of ionization of the lone-pair electrons (of H_nX) when such electrons are available. The stability of the Rydberg XH_{n+1} radicals is proportional to the proton affinity of XH_n.* In accord, the stability of a hypercoordinated radical (relative to $XH_n + H^{\bullet}$) is predicted to increase down a column of the periodic table and to peak at the Vth family of each period (**26**). These principles are applied to systems that have been investigated experimentally and computationally: SiH_5, PH_4, SH_3, CH_5, NH_4, and OH_3. UHF-SCF/6-31G* calculations are performed and VB weight analysis is carried out to assess the stability and electronic structure of SiH_5, PH_4, and SH_3. It is concluded that SiH_5, CH_5, and SH_3 are transition states typified by delocalized three-electron three-center (3e,3c) bonding. On the other hand, PH_4 is either a metastable intermediate (**2**) or a stable species (**1**) that is described by roughly equal contributions from (3e,3c) and (4e,3c) bonding. Finally, NH_4 and OH_3 are metastable intermediates with a decreasing stability and a Rydberg character. Prediction are made about the chances of finding other stable hypercoordinated XH_{n+1} radicals.

Two alternative models are generally invoked to account for the origins of bonding in hypercoordinated molecules.[1-3] The first model advocates hypervalency and relies on sp^3d^n (n greater than or equal to 1) hybridizations to generate the necessary number of bond orbitals that are required to accommodate more than four electron pairs around the hypervalent atom.[3] This model accounts successfully for the general observation that hypervalency is associated more with second- (third, etc.) row rather than with first-row atoms.[1] The second model utilizes MO theory and ascribes the hypercoordination to a "Rundle-three-center" bonding.[4] This second model is more economical, in the sense that shell expansion is avoided and d orbitals are not required for describing the hypercoordination. While the Rundle MO model explains the bonding in hypercoordinated compounds, it does not account in a lucid manner for the predominance of hypercoordination among second- (third, etc.) row atoms. However, the recent syntheses of hypercoordinated compounds of carbon,[5] oxygen,[6] and fluorine[7] favor the approach that hypercoordination need not derive from the hypervalency associated with d orbitals on the hypercoordinated atom.[8] A concensus is gradually forming that d orbitals are not part of the valence shell of the hypercoordinated atom though these orbitals may assist bonding by polarizing the valence s and p atomic orbitals of the hypercoordinated atom.[9]

While the hybridization and MO models can each describe the bonding features of the normal-valent and hypervalent or hypercoordinated species, these models cannot a priori predict the relative stability of the two species. This is the very insight which is within the reach of the valence bond (VB) curve-crossing diagram model.[10-13] This insight has recently been demonstrated, by some of us,[14] by analyzing the stability of (10–S–4)[8b] sulfuranes R_2SX_2 relative to their localized constituents, $X^- + R_2S^+–X$, as a function of the ligand X. In fact, a variety of hypercoordination problems have been already analyzed with the VB model, though the designation of these problems as reactivity[10] or delocalization[13] did not reveal their inherent link to hypercoordination. It appears

[†] Université de Paris-Sud.
[‡] Ben Gurion University.

(1) Musher, J. I. *Angew. Chem., Int. Ed. Engl.* **1969**, *8*, 54.
(2) Kutzelnigg, W. *Angew. Chem., Int. Ed. Engl.* **1984**, *23*, 272, and references therein.
(3) Coulson, C. A. *Nature* **1969**, *221*, 1106. Brill, T. B. *J. Chem. Educ.* **1973**, *50*, 392.
(4) Rundle, R. E. *J. Am. Chem. Soc.* **1963**, *85*, 112. Hoffmann, R.; Howell, J. M.; Muetterties, E. L. *J. Am. Chem. Soc.* **1972**, *94*, 3047. Chen, M. M. L.; Hoffmann, R. *J. Am. Chem. Soc.* **1976**, *98*, 1647.
(5) (a) Forbus, T. R.; Martin, J. C. *J. Am. Chem. Soc.* **1979**, *101*, 5057. (b) Schleyer, P. v. R.; Würthwein, E. U.; Clark, T. *J. Am. Chem. Soc.* **1983**, *105*, 5930.
(6) Schleyer, P. v. R.; Würthwein, E. U. *J. Am. Chem. Soc.* **1982**, *104*, 5839. Wu, C. H. *Chem. Phys. Lett.* **1987**, *139*, 357.
(7) Cahill, P. A.; Dykstra, C. E.; Martin, J. C. *J. Am. Chem. Soc.* **1985**, *107*, 6359. Ault, B. S.; Andrews, L. *Inorg. Chem.* **1977**, *16*, 2024.
(8) (a) For leading references on hypervalency see: Martin, J. C. *Science* **1983**, *221*, 509. Perkins, C. W.; Clarkson, R. B.; Martin, J. C. *J. Am. Chem. Soc.* **1986**, *106*, 3206. Perkins, C. W.; Martin, J. C. *J. Am. Chem. Soc.* **1986**, *106*, 3211. For a discussion of the terms hypervalency and hypercoordination, see: Schleyer, P. v. R.; Martin, J. C. *Chem. Eng. News* **1984**, May 28, 4. Schleyer, P. v. R. Hypervalency Symposium 191st ACS National Meeting, New York, April, 1986; Abstract ORGN 117. (b) In our paper, we prefer the term hypercoordination in conjunction with Martin's nomenclature; see: Perkins, C. W.; Martin, J. C.; Arduengo, A. J.; Lau, W.; Alegria, A.; Kochi, J. K. *J. Am. Chem. Soc.* **1980**, *102*, 7753.
(9) Wolfe, S.; LaJohn, L. A.; Bernardi, F.; Mangini, A.; Tonachini, G. *Tetrahedron Lett.* **1983**, *24*, 3789. Wolfe, S.; Stolow, A.; LaJohn, L. A. *Ibid.* **1983**, *24*, 4071. Schleyer, P. v. R.; Clark, T.; Kos, A. J.; Spitznagel, G. W.; Rohde, C.; Arad, D.; Houk, K. N.; Rondan, N. G. *J. Am. Chem. Soc.* **1984**, *106*, 6467.
(10) (a) Shaik, S. S. *J. Am. Chem. Soc.* **1981**, *103*, 3692. (b) Shaik, S. S. *Prog. Phys. Org. Chem.* **1985**, *15*, 197.
(11) Pross, A.; Shaik, S. S. *Acc. Chem. Res.* **1983**, *16*, 363.
(12) Pross, A.; Shaik, S. S. *J. Am. Chem. Soc.* **1982**, *104*, 187.
(13) (a) Shaik, S. S.; Bar, R. *Nouv. J. Chim.* **1984**, *8*, 411. (b) Shaik, S. S.; Hiberty, P. C. *J. Am. Chem. Soc.* **1985**, *107*, 3089. (c) Shaik, S. S.; Hiberty, P. C.; Lefour, J. M.; Ohanessian, G. *J. Am. Chem. Soc.* **1987**, *109*, 363. (d) Shaik, S. S.; Hiberty, P. C.; Ohanessian, G.; Lefour, J. M. *Nouv. J. Chim.* **1985**, *9*, 385. (e) Shaik, S. S.; Hiberty, P. C.; Ohanessian, G.; Lefour, J. M. *J. Phys. Chem.* **1988**, *92*, 5086.
(14) Volatron, F.; Eisenstein, O. *J. Chem. Soc., Chem. Commun.* **1986**, 301.

0002-7863/89/1511-5623$01.50/0

thus that the VB model can serve as a general framework with which to conceptualize and pattern data associated with this particular aspect of the hypercoordination/hypervalency question.

The present paper uses the VB approach to analyze (9–X–(n+1)) hypercoordinated radicals of the general formula XH_{n+1} (X = C, N, O, Si, P, S). The index n + 1 signifies that the coordination shell of the atom X contains an additional hydrogen atom relative to the normal-valent molecule, XH_n.

The analysis focuses on two main aspects of the problem. The first aspect is concerned with the stability of the hypercoordinated species, relative to its normal-valent constituents, as a function of the central atom X. Three classes of hypercoordinated compounds and their origins will be discussed, as outlined in **1**–**3**. The second aspect deals with the possible variation of the bonding character of the hypercoordinated species as a function of the atom X.

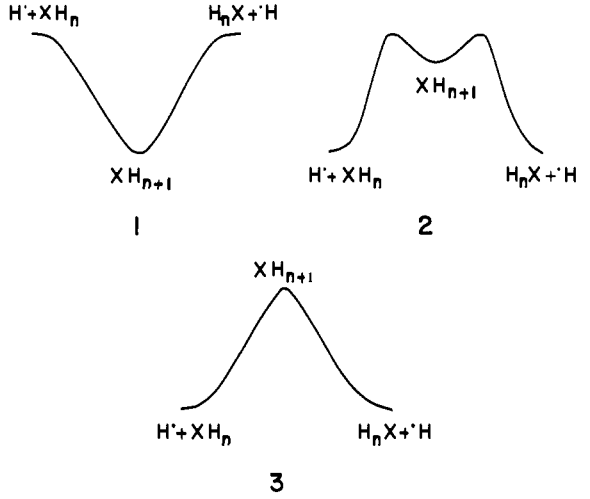

Previous Studies

Let us first recall the theoretical and experimental studies concerning these species. PH_4 has been observed in various matrices by several groups[15-17] and was shown to be stable up to 122 K.[16] Numerous ab initio calculations[18-21] have shown that PH_4 possesses a distorted trigonal bipyramidal structure with a missing ligand at the equatorial position (TBPe) as depicted in **4**. Though the odd electron is drawn to be localized on phosphorus, significant odd electron density is found[20,21] to reside on the axial positions so that structure **5** is equally "correct", with dashed lines signifying three-electron three-center (3e,3c)-bonding.[8] It is as yet unclear whether PH_4 is a stable species as **1** or a metastable intermediate as in **2**.

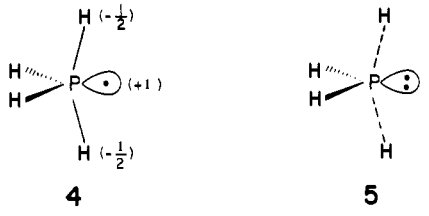

The presence of SiH_5 and GeH_5 in various matrices has been recently postulated.[22] Also, SiH_5 had been previously invoked[23] as an intermediate to rationalize kinetic results concerning the reaction H + SiH_4. On the other hand, ab initio calculations[24] predict SiH_5 to be higher in energy than the normal-valent constituents, SiH_4 + H, that is, a species such as **3** or possibly **2**.

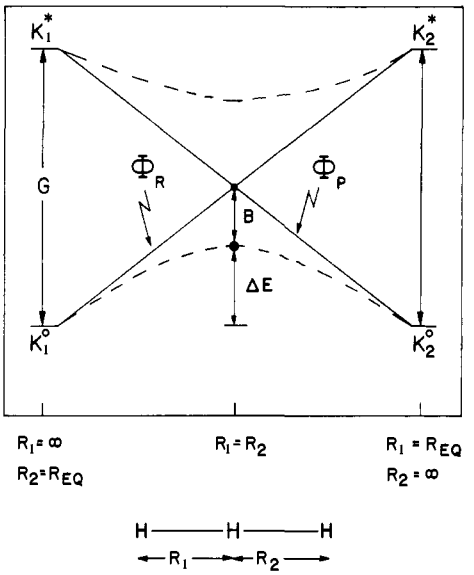

Figure 1. Curve-crossing diagram for H' + H_2 → [H_3] → H_2 + H'. The Lewis curves are denoted by Φ_R and Φ_P, and their avoided crossing by a dashed line. The hypercoordinated (3–H–2) species, H_3, lies above its normal-valent constituents by ΔE. The diagram is applicable to any (3–X–2), (9–X–5) or (9–X–3) species that can be described mainly by (3e,3c) bonding. The X-dependent variables are G, B, and the final ΔE (see **8** → **9**).

To our knowledge, the radical SH_3 has never been observed. Ab initio calculations carried out by some of us have shown[25] that this structure is metastable like **2** but with an extremely tiny barrier for decomposition to SH_2 + H.

The stability of the NH_4 radical in its ground state is still controversial.[26] Herzberg[27] determined the spectrum of the Rydberg excited state of NH_4 and suggested its ground state (GS) to be dissociative. On the other hand, the GS of ND_4[28] and that of the clusters $(NH_3)_n(NH_4)$[29] have been observed. Theoretical calculations[30-33] confirm this low stability and assign NH_4 a GS of a Rydberg type that is almost isoenergetic with the normal-valent products NH_3 + H with a barrier of about 10 kcal/mol separating NH_4 and NH_3 + H.

The OH_3 radical displays a similar behavior. The GS of OH_3 has been observed only for the deuterated species OD_3 or for the cluster $(OH_2)_n(OH_3)$.[34] Ab initio calculations[35,36] confirm, as

(15) McDowell, C. A.; Mitchell, K. A. R.; Raghunathan, P. *J. Chem. Phys.* **1972**, *57*, 1699. Claxton, T. A.; Fullam, B. W.; Platt, E.; Symons, M. C. R. *J. Chem. Soc., Dalton Trans.* **1975**, 1395.
(16) Colussi, A. J.; Morton, J. R.; Preston, K. F. *J. Chem. Phys.* **1975**, *62*, 2004; *J. Phys. Chem.* **1975**, *79*, 1855.
(17) Shimokoshi, K.; Nakamura, K.; Sato, S. *Mol. Phys.* **1984**, *53*, 1239.
(18) Howell, J. M.; Olsen, J. F. *J. Am. Chem. Soc.* **1976**, *98*, 7119.
(19) Hudson, A.; Treweek, R. F. *Chem. Phys. Lett.* **1976**, *39*, 248.
(20) Janssen, R. A. J.; Visser, G. J.; Buck, H. M. *J. Am. Chem. Soc.* **1984**, *106*, 3429. Janssen, R. A. J.; Buck, H. M. *J. Mol. Struct. (THEOCHEM)* **1984**, *19*, 139.
(21) Gonbeau, D.; Guimon, M. F.; Ollivier, J.; Pfister-Guillouzo, G. *J. Am. Chem. Soc.* **1986**, *108*, 4760.
(22) SiH_5: Nakamura, K.; Masaki, N.; Sato, S.; Shimokoshi, K. *J. Chem. Phys.* **1985**, *83*, 4504. GeH_5: Nakamura, K.; Masaki, N.; Okamoto, M.; Sato, S.; Shimokoshi, K. *Ibid.* **1987**, *86*, 4949.
(23) Glasgow, L. C.; Olbrich, G.; Potzinger, P. *Chem. Phys. Lett.* **1972**, *14*, 466.
(24) Thuraisingham, R. A. *Ind. J. Chem.* **1979**, *18A*, 509.
(25) Volatron, F.; Demolliens, A.; Lefour, J. M.; Eisenstein, O. *Chem. Phys. Lett.* **1986**, *130*, 419.
(26) Wan, J. K. S. *J. Chem. Educ.* **1968**, *45*, 40.
(27) Herzberg, G. *Faraday Discuss. Chem. Soc.* **1981**, *71*, 165.
(28) Gellene, G. I.; Cleary, D. A.; Porter, R. F. *J. Chem. Phys.* **1982**, *77*, 3471. Whittaker, E. A.; Sullivan, B. J.; Bjorklund, G. C.; Wendt, H. R.; Hunziker, H. E. *J. Chem. Phys.* **1984**, *80*, 961.
(29) Gellene, G. I.; Porter, R. F. *J. Phys. Chem.* **1984**, *88*, 6680. Jeon, S.-J.; Raksit, A. B.; Gellene, G. I.; Porter, R. F. *J. Am. Chem. Soc.* **1985**, *107*, 4129.
(30) McMaster, B. N.; Mrozek, J.; Smith, V. H. *Chem. Phys.* **1982**, *73*, 131.
(31) Cardy, H.; Liotard, D.; Dargelos, A.; Poquet, E. *Chem. Phys.* **1983**, *77*, 287.
(32) Kaspar, J.; Smith, V. H.; McMaster, B. N. *Chem. Phys.* **1985**, *96*, 81.
(33) Kassab, E.; Evleth, E. M. *J. Am. Chem. Soc.* **1987**, *109*, 1653.
(34) Gellene, G. I.; Porter, R. F. *J. Chem. Phys.* **1984**, *81*, 5570.
(35) Gangi, R. A.; Bader, R. F. W. *Chem. Phys. Lett.* **1971**, *11*, 216.
(36) Niblaeus, K. S. E.; Ross, B. O.; Siegbahn, P. E. M. *Chem. Phys.* **1977**, *25*, 207.

in the NH_4 case, that OH_3 is a metastable compound with a Rydberg ground state, less stable than the normal-valent products by about 20 kcal/mol, and separated from them by a barrier of nearly 5 kcal/mol. Thus, both NH_4 and OH_3 belong to the general class **2** but are Rydberg-hypercoordinated species.

The CH_5 radical has never been observed experimentally. Theoretical ab initio calculations[37,38] indicate that CH_5 is likely to be the transition state (TS) for the H-exchange reaction in CH_4 as depicted by the general class **3**.

In summary, the known XH_{n+1} radicals exhibit a spectrum of behaviors that, depending on the central atom, range between the extremes **1** and **3**. PH_4 is a true minimum, of the types **1** or **2**. On the other hand, CH_5 and SH_3 appear by theoretical means to be of the type described by **3**. Experimental results suggest that SiH_5 is a minimum (i.e., either **1** or **2**) while theory predicts this radical to be unstable with respect to dissociation (**3** or **2**). Finally, both OH_3 and NH_4 can be classified as **2** with NH_4 being the more stable structure. In what follows we attempt to understand these trends and to outline thereby a general theory for hypercoordinated XH_{n+1} radicals.

Qualitative Analysis

A. Valence Bond Model for Hypercoordinated XH_{n+1} Species. The method is based on curve-crossing diagrams that have been used for the study of the S_N2 reaction.[10,11] This approach has been shown fruitful in the analysis of X_3 hypercoordinated species,[13] where X is a monovalent one-electron atom or group. For clarity, we briefly summarize the principles of the method, using as an example the reaction $H + H_2 \rightarrow H_2 + H$ in which (H–H–H) is a hypercoordinated (3–H–2) species. The curve-crossing diagram is displayed in Figure 1, where the geometric deformation of the H_3 supersystem is recorded in the abscissa. The left-hand side of the diagram corresponds to the geometry of the reactants, i.e., a hydrogen atom infinitely far from a hydrogen molecule, and the right-hand side corresponds to that of the products. The middle of the abscissa in the locus of the hypercoordinated geometry.

The electronic states of the reactants and products can each be described by a single VB function, whose energy is plotted by using a full line as a function of the geometry of the supersystem. For example, the curve Φ_R, which is associated with the VB function describing the reactants, has its minimum at left-hand side ($K°_1$) of the diagram and gradually rises in energy as one goes from left to right in the diagram, i.e., from reactant to product geometry. The curve Φ_R thus connects $K°_1$, the reactant's ground state, to a state K^*_2, which can be described as the image of the reactants in the product geometry.[13b] Thus, $K°_1$ and K^*_2 correspond respectively to the VB structures **6** and **7**, in which the solid line represents the singlet coupling of the electrons, while the short H···H distance is indicated by the parentheses to emphasize the geometric distinction between the structures.

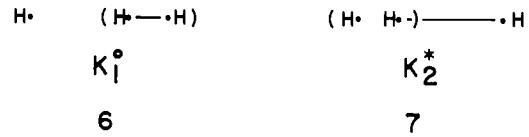

It should be noted that in the way defined here, K^*_2 is not a spectroscopic excited state of the products,[39a] but it can be shown[13c] that it lies above the GS by an energy-gap quantity G, which is related to a spectroscopic state:

$$G = \tfrac{3}{4}\Delta E_{ST} \quad (1)$$

Here ΔE_{ST} is the first vertical singlet–triplet transition energy of the hydrogen molecule. Thus, it is convenient to represent K^*_2 in **7** as a hydrogen atom far from a hydrogen molecule that is excited into its triplet state. In a similar way, curve Φ_P connects the GS $K°_2$ of the products to the state K^*_1, the image of the products in the reactant geometry.

Now the VB functions Φ_R and Φ_P constitute a nearly complete basis[39b] of VB structures to describe any point of the H_3 GS surface, and thus the adiabatic reaction profile, represented in dotted line is the result of the variational mixing of the VB functions Φ_R and Φ_P. Consequently, at the anchor points the GS adiabatic curve merges with the states $K°_1$ and $K°_2$, which are respectively the GS of the reactants and products, while in the hypercoordinated region, the mixing between Φ_R and Φ_P results in a stabilization which is indicated by B in the diagram. Hereafter, Φ_R and Φ_P will be referred to as the Lewis curves to emphasize their relation to the Lewis type bonding (normal-valent) of $K°_1$ and $K°_2$.

After avoided crossing the reaction profile may display either a transition state or a minimum. Referring, as an example, to cases that differ mostly in their energy gaps (G), then a large gap in the one extreme will lead to a transition state, hypercoordinated species such as in **8**, while a very small gap will result, after avoided crossing, in a stable hypercoordinated species as described in **9**.[13]

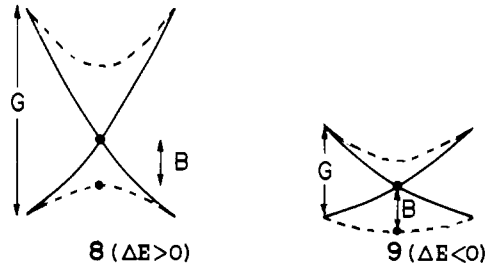

The relationship can be expressed quantitatively as follows:

$$\Delta E = fG - B \quad (2)$$

Here ΔE is the energy of the hypercoordinated species relative to its normal-valent constituents, $X_2 + X$. The factor fG is the height of the crossing point (relative to $X_2 + X$) expressed as some fraction (f) of the diagram gap, G. The factor B is the mixing or resonance energy at the crossing point. Thus, the stability of the hypercoordinated species relative to its normal-valent constituents is determined by an interplay of the three factors in eq 2.

For some hypercoordinated trimers (3–X–2), some of us have recently evidenced a correlation between ΔE and G (ΔE_{ST}).[13b,c] Thus, large ΔE_{ST} values resulted in unstable hypercoordinated trimers such as **8** ($\Delta E > 0$), while very small ΔE_{ST} values resulted in stable hypercoordinated trimers such as **9** ($\Delta E < 0$). The observation of such a general correlation means that G is the dominant variable in eq 2, while f and B vary either in the same direction as G[13e] or less significantly. In such series, the hypercoordinated species is expected to exhibit a spectrum of stability between the extremes **8** and **9**.[13] The organizing quantity of this series will be G, while is related to ΔE_{ST} (eq 1), which, in turn, is related to the bond energy of the normal-valent dimer X_2. Thus, *the stability of the hypercoordinated species in such a series is expected to correlate with the weakness of the bond in the normal-valent molecule.* This is one kind of correlation that we will be looking for in the hypercoordinated radicals XH_{n+1}.

Some cases may be more complicated than Figure 1 because more VB structures contribute to the description of the supersystem.[11,12] The choice of such functions always obeys a very simple rule: all the VB functions contributing to the supersystem's GS, at any point of the potential surface, must be included in the diagram. Especially interesting are the cases where the additional VB structures mix into the hypercoordinated geometry but not into the ground states of the normal-valent structures. The final result of the avoided crossing depends on the proximity of these intermediate VB structures (Φ_I) to the crossing point of the two Lewis curves.[40] Typically, these intermediate structures involve

(37) Morokuma, K.; Davis, R. E. *J. Am. Chem. Soc.* **1972**, *94*, 1060.
(38) Niblaeus, K. S. E.; Roos, B. O.; Siegbahn, P. E. M. *Chem. Phys.* **1977**, *26*, 59.
(39) (a) An alternative is to let K^*_2 correlate with the real state of H plus a triplet H_2; see, e.g., ref 13a. (b) This is true if Φ_R and Φ_P are both multistructure VB functions, in which, in particular, the ionic/covalent ratio of the formal bond is variationally optimized. For leading references on such VB calculations, see: van Lenthe, J. H.; Balint-Kurti, G. G. *J. Chem. Phys.* **1983**, *78*, 5699.

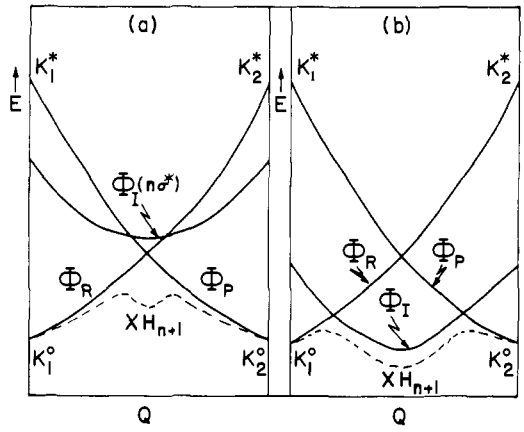

Figure 2. Curve-crossing diagram for cases where X possesses a lone pair. The intermediate configuration Φ_I involves, in general, an $(n \rightarrow \sigma^*)$ excitation relative to the Lewis curves. (a) The intermediate curve lies close to the Φ_R–Φ_P intersection but still above it. The result is a metastable hypercoordinated species. (b) Φ_I crosses Φ_R and Φ_P below their crossing point. The resulting hypercoordinated species is more or as stable as its normal-valent constituents. This species possesses a major $(n \rightarrow \sigma^*)$ electronic character.

excited "states" that do not correlate with the GS reactants and products and that correlate horizontally across the diagram.[40] Sources for such intermediate configurations, in the present problem of XH_{n+1} radicals, are charge-transfer states and various local excitations on the central atom, involving orbitals that do not partake in the bond breaking–making process.

In the general case, the mixing of the intermediate configurations into the Lewis curves (Φ_R and Φ_P) will further stabilize the hypercoordinated species so that even a large gap, G, may result in a hypercoordinated species that is only slightly dissociative relative to the normal-valent constituent.

In special cases when the intermediate VB structure is very stable, the hypercoordinated species may become a metastable intermediate or a stable species even if the gap, G, is not small. These cases are illustrated in Figure 2 and account for the metastable species depicted in **2**. In both cases, the hypercoordinated state will acquire a major character of the intermediate configuration, so that the bonding mechanism of the hypercoordinated states of Figures 1 and 2 will be distinct.

What remains is to identify for each particular case the low-lying intermediate configurations that are likely to contribute to the hypercoordinated species. This can be done quite simply by utilizing available thermochemical quantities such as bond energies, ionization potentials, electron affinities, and so on.

B. Application to SiH_5, PH_4, and SH_3. Let us consider SiH_5 as an intermediate structure of the H exchange in SiH_4, as depicted in **10**. If we assume that the electrons of the equatorial Si–H

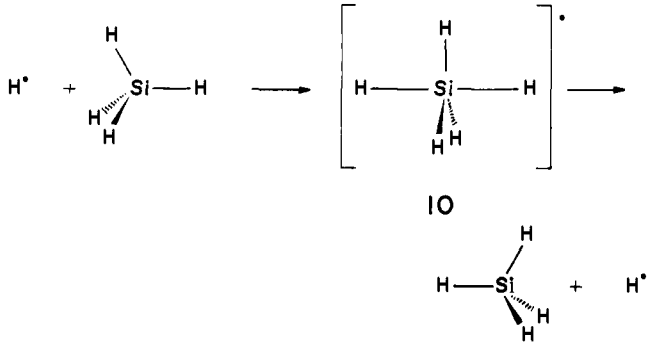

10

bonds are not "active" or do not participate in the reaction, the problem is reduced to a system involving three electrons and three orbitals: two atomic 1s orbitals of the axial hydrogens and one orbital of the Si atom. The latter orbital is a pure p at the hypercoordinated geometry and gradually hybridizes upon moving toward the reactants or the products. Therefore the same diagram as in the H_3 case can be drawn for this reaction. There are no intermediate configurations that are low enough to mix significantly into the hypercoordinated structure so that the case of SiH_5 is described, as in Figure 1, by avoided crossing of two Lewis curves (Φ_R, Φ_P).

Like SiH_5, PH_4 too, may be considered as a structure in the course of the exchange reaction **11**. As we shall see though, PH_4

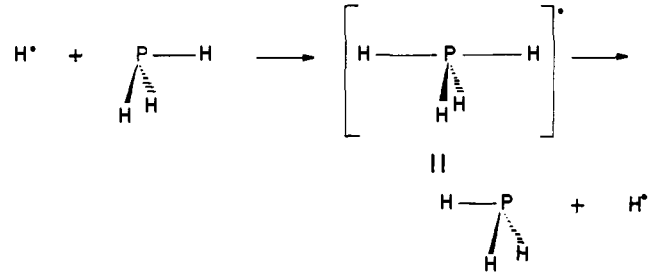

11

and SiH_5 are qualitatively different. Let us, in a first step, treat PH_4 like SiH_5 and consider that the lone pair and the two P–H bonds which become equatorial in the hypercoordinated region are unaffected throughout the reaction. The reacting system is thus reduced to three electrons and three orbitals: the AOs of the incoming and departing hydrogens and a p-type orbital on phosphor. The corresponding VB correlation diagram should then be equivalent to Figure 1 with two intersecting Lewis curves, leading thereby to a hypercoordinated species that is represented by the resonating VB scheme **12**.

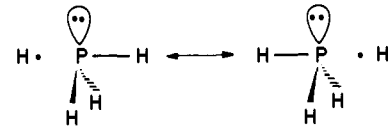

12

However by restricting ourselves to VB configurations that describe properly the normal-valent species, H + PH_3, we miss some important intermediate configurations that mix only into the hypercoordinated region as described in Figure 2. These intermediate configurations derive from the involvement of the phosphorus lone-pair hybrid, in the electronic reorganization.

Consider **13** and **14**, which are symmetrized VB configurations that involve lone-pair reorganizations by shifting an electron from

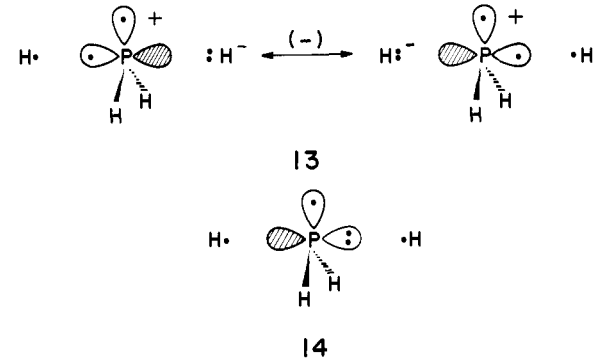

13

14

the lone pair either to one of the hydrogens (**13**) or to the axial p orbital on phosphorus (**14**). **13** is itself a combination of two structures, whose relative orbital weights are equal at the symmetrical geometry and unequal at the extremities of the diagram.

At the reactant and product geometries, **13** and **14** are mixed and correspond to the $(n \rightarrow \sigma^*)$ excited configurations **15** and **16**. Thus, the anchor states of the intermediate configuration, Φ_I (Figure 2), correspond in the case of H + PH_3 to the (bond-localized) $(n \rightarrow \sigma^*)$ states of PH_3. The relative contributions of **13** and **14** to the intermediate curve, Φ_I, vary with the geometry of the PH_4 supersystem. At the hypercoordinated geometry the

(40) See ref 10b, pp 204–206.

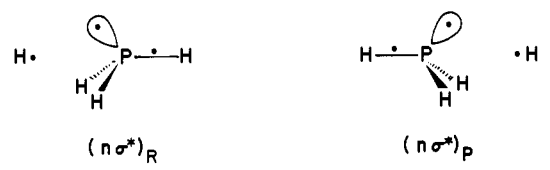

15 **16**

VB configuration **13** involves P···H axial (3e,3c) bonding as well as electrostatic stabilization. On the other hand, **14** is devoid of both stabilizing effects. These features would favor a greater character of **13** in the intermediate curve, Φ_1, near the hypercoordinated region.

To summarize, the intermediate curve for the PH_4 supersystem has a character of ($n \rightarrow \sigma^*$) excitation that involves mixing of **13** and **14** in variable proportions. Near the hypercoordinated geometry this curve mixes into the intersection point of the reactant and product curves and as shown in Figure 2, the hypercoordinated state will thereby be stabilized. A quantitative analysis is required to decide whether the actual situation in PH_4 is indeed like Figure 2a or Figure 2b, or alternatively the ($n \rightarrow \sigma^*$) is too high-lying and unimportant. Quantitative VB weight analyses are required to answer this question and are discussed later.

The analysis of SH_3 follows the exact same lines. Here too the lone pair on sulfur partakes in the electronic reorganization and an ($n \rightarrow \sigma^*$) curve—made up of **13**-like and **14**-like configurations—mixes in to stabilize the hypercoordinated state.[41]

The energy of the ($n \rightarrow \sigma^*$) curve depends critically on the lone-pair ionization potential of the central atom IP_X: the lower the IP_X, the greater the stabilization enjoyed by the hypercoordinated structure. Since the lone-pair ionization potential is larger for SH_2 than for PH_3 (306 vs 244 kcal/mol),[42] we expect the ($n \rightarrow \sigma^*$) curve to be more influential in stabilizing PH_4.

Theoretical Calculations and Discussion

A. SCF Computations and a Comparison of SiH_5, PH_4, and SH_3. To provide a quantitative aspect to the above analysis, we calculated the three title species by means of ab initio calculations of UHF type, in 6-31G* basis set,[43] using the MONSTERGAUSS program.[44] Geometry optimizations have been carried out through an analytical gradient method. The results are reported in Figure 3.

Table I shows the calculated energies of the hypercoordinated species relative to their normal-valent constituents. The values are denoted as ΔE and are shown alongside the experimental bond energies in the normal-valent XH_n molecules. As may be seen, all the ΔE values are positive, indicating more stable normal-valent constituents (XH_n + H) at the employed computational level.

The SCF ΔE results may be interpreted by discussing the trends in the bond energies and the lone-pair ionization potentials. The strongest bonds are those of Si–H (90.3 kcal/mol)[45] and S–H (87.7 kcal/mol),[46] which should lead to equivalent ΔE for SiH_5 and SH_3. Since the P–H bond is weaker (76.7 kcal/mol),[46] a smaller ΔE

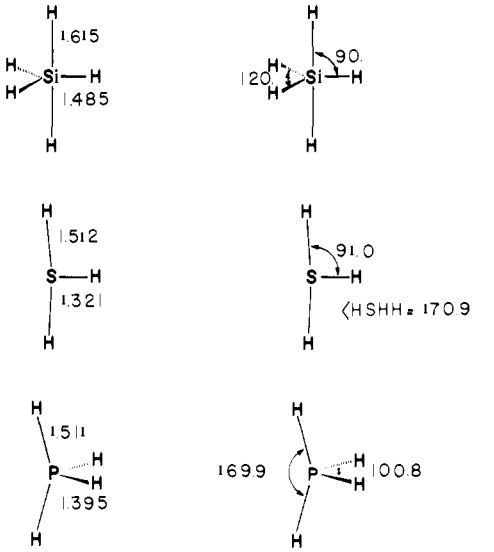

Figure 3. Optimized structures (UHF/6-31G*) for SiH_5, PH_4, and SH_3. Bonds are in angstroms, and angles in degrees.

Table I. Experimental X-H Bond Energies[45,46] (D_{X-H}) in the XH_n Molecules and Calculated Stability of the XH_{n+1} Radical (ΔE)[a]

	Si	P	S
D_{X-H}	90.3	76.7	87.7
ΔE	31.8	6.0	22.7

[a] All quantities are in kcal/mol.

is expected for PH_4. If we now take into account the added influence of the ($n \rightarrow \sigma^*$) configuration, ΔE should be lowered for both PH_4 and SH_3 in comparison with SiH_5. Now since IP_X is lower for PH_3 than for SH_2,[42] the PH_4 species should be by far the most stable one among these species. Overall, the following ΔE order is predicted in full agreement with ab initio results:

$$\Delta E(SiH_5) > \Delta E(SH_3) \gg \Delta E(PH_4)$$

As a consequence, both PH_4 and SH_3 cases behave qualitatively like in Figure 2a, in which the mixing of the intermediate configuration creates a metastable hypercoordinated intermediate species. However, in the case of SH_3 the ($n \rightarrow \sigma^*$) curve is high lying and, while ($n \rightarrow \sigma^*$) mixes into the crossing point, the mixing is insufficient to endow the metastable intermediate with any sizeable stability.[25]

To verify this final conclusion, the MO wave functions of PH_4 and SH_3 have been reexpressed in terms of VB structures.[47] The relative weights of (3e,3c) configuration (e.g., **12**) and the two ($n \rightarrow \sigma^*$)-type configurations (e.g., **13** and **14**) are shown in **17**

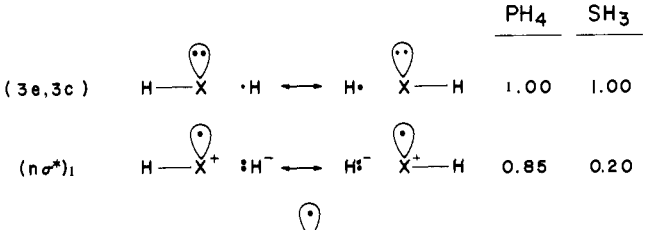

17

for the two hypercoordinated species. As may be seen, the ($n \rightarrow \sigma^*$) configurations for PH_4 possess jointly, approximately the same weight as the (3e,3c) configuration. On the other hand, for SH_3

(41) Since SH_2 possesses two (n and 2p) lone pairs, two intermediate curves ($n \rightarrow \sigma^*$) and ($2p \rightarrow \sigma^*$) may be initially considered for SH_3. The SH_3 radical is almost planar, and hence the ($2p \rightarrow \sigma^*$) configuration is almost orthogonal to the ground state and cannot be involved in our VB correlation diagram. A more detailed comparison of the electronic structure of sulfuranyl radicals will be published elsewhere: Demolliens, A.; Volatron, F., in preparation.

(42) (a) *Gas Phase Ion Chemistry*; Bowers, M. T. Ed.; Academic Press: New York, 1979; Vol. 2, p 17 (for PH_3). (b) Turner, D. W.; Baker, C.; Baker, A. D.; Brundle, C. R. *Molecular Photoelectron Spectroscopy*; Wiley: London, 1970 (the IP of the *n* lone pair of H_2S).

(43) For first-row atoms: Hehre, W. J.; Ditchfield, R.; Pople, J. A. *J. Chem. Phys.* **1972**, *56*, 2257. Hariharan, P. C.; Pople, J. A. *Theor. Chim. Acta* **1973**, *28*, 213. For second-row atoms: Gordon, M. S.; Binkley, J. S.; Pople, J. A.; Pietro, W. J.; Hehre, W. J. *J. Am. Chem. Soc.* **1982**, *104*, 2797. Francl, M. M.; Pietro, W. J.; Hehre, W. J.; Binkley, J. S.; Gordon, M. S.; DeFrees, D. J.; Pople, J. A. *J. Chem. Phys.* **1982**, *77*, 3654.

(44) MONSTERGAUSS: Poirier, R. A.; Peterson, M. R. Department of Chemistry, University of Toronto, Canada, 1981.

(45) Doncaster, A. M.; Walsh, R. *Int. J. Chem. Kinet.* **1981**, *13*, 503. Walsh, R. *Acc. Chem. Res.* **1981**, *14*, 246.

(46) Sanderson, R. T. *Polar-Covalence*; Academic Press: New York, 1983; pp 46–48.

(47) We have used a program projecting the SCF wave function on a basis of VB structures, as described in: Hiberty, P. C.; Leforestier, C.; *J. Am. Chem. Soc.* **1978**, *100*, 2012. So as to reduce the computation to a minimal number of electrons and orbitals, we previously localized the molecular orbitals by using the usual Boys method. For more details on the projection technique in double-ζ basis set, see: Hiberty, P. C.; Ohanessian, G. *J. Am. Chem. Soc.* **1982**, *104*, 66.

the (n → σ*) configurations constitute a minor fraction of the total wave function. These results are in line with the expectations based on the relative lone-pair ionization potentials. The curve-crossing situations can be summarized, then, as shown schematically in **18** and **19**.

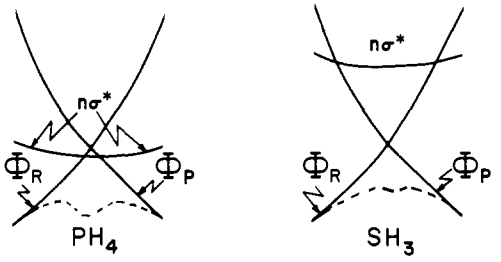

18 **19**

It should be noted that the ground-state energy curve of SH_3 (dotted lines in **19**) displays a very shallow potential well of nearly 1 kcal/mol at the UHF-4-31G* level.[25] This result, confirmed at the CI level,[25] is in harmony with the marginal role played by the (n → σ*) configuration in weakly stabilizing the hypercoordinated structure.

B. Bonding and Structural Analysis. There is another way to represent the bonding in a pictorial manner which resembles the MO representation. This method[48] utilizes the Slater determinants of the VB representation to construct symmetry-adapted linear combinations. The result for (3c,3e) bond as in SiH_5 is a bond diagram, **20**, that describes the electron pairing between the central

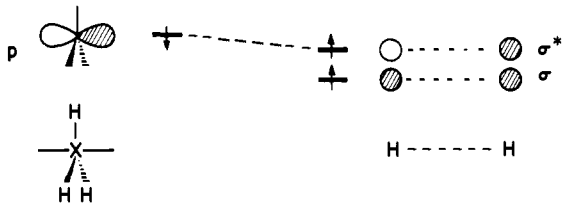

20 **(1 BOND - PAIR)**

atom, as one fragment, and the two axial hydrogens, as the second fragment. Thus there exists one bond pair between the central atom and the two axial hydrogens. This bond pair is shown by the dashed line in **20** and involves a pair of spin-coupled electrons, one residing on the p orbital of the XH_3 fragment and the other in a σ*-type orbital of the axial H···H fragment.[49] An additional odd electron resides in a σ-type orbital of the H···H fragment. Thus, the bond diagram utilizes the Heitler–London bond pairing[49] with fragment orbitals rather than atomic orbitals. A very similar fragment VB bonding scheme can be drawn for the (3e,3c) component contributing to the PH_4 electronic structure (see **21**). It involves a Heitler–London bond pairing between one electron on the 3p orbital of P and the σ* orbital on the H···H fragment, while two electrons stand in the n orbital.

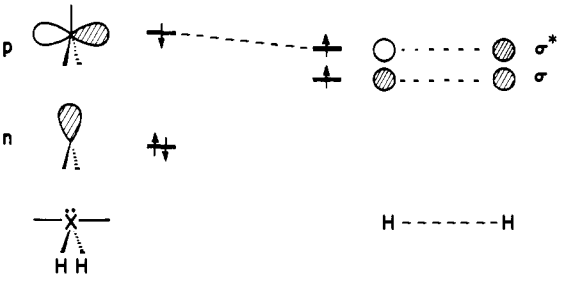

21

The bonding features are also affected by the involvement of the (n → σ*) configurations. As seen in **13**, the dominant (n → σ*) configuration is the one involving charge transfer from the lone pair to the axial hydrogens. The bonding features of this configuration are better revealed by using a bond diagram that is shown in **22** and is seen to derive from the (3e,3c) configuration,

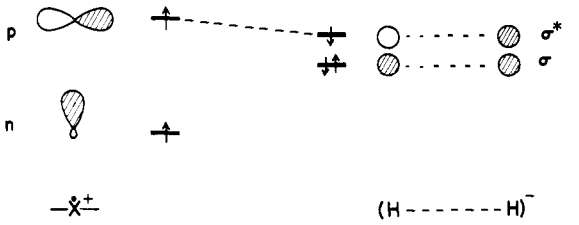

22

21, by a one-electron shift from the lone pair hybrid to the σ-like hydrogenic fragment orbital. The configuration possesses accordingly one bond pair (p–σ*, in dashes) that connects the hypercoordinated atom to axial hydrogens[50] and a negative charge distributed on the hydrogens. This description fits the definition of (4e,3c) bonding.

In SH_3, **22** contributes only slightly to the bonding, and it is possible to approximate SH_3 by a **21**-like bond diagram that involves (3e,3c) bonding. A compact representation of the situation may be given by **23** in which the dashed line represents (3e,3c) bonding and the full line (2e,2c) bonding.

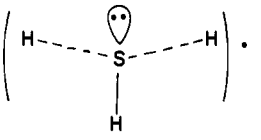

23

In PH_4 there are roughly equal contributions of **21** and **22** to the bonding as shown in **24**. The bonding is still sustained by

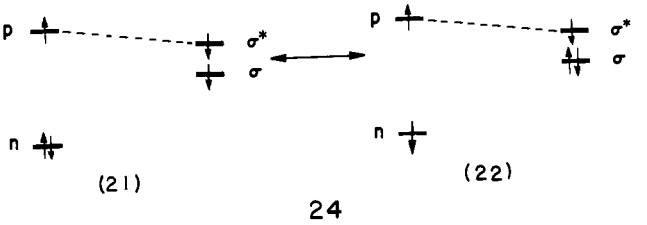

24

a single-bond pair, but a major reorganization has occurred due to the lone-pair involvement. With use of compact pictures, this can be represented by **25**.

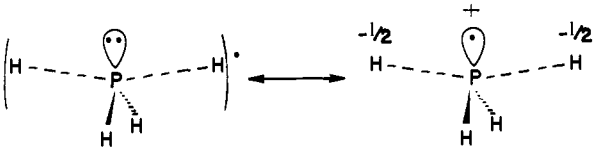

25

A factor that contributes to bonding and that cannot be shown pictorially, in either **24** or **25** is the resonance interaction between the two major configurations that contribute to PH_4. Inspection of **24** reveals that the two configurations differ by a shift of one electron between the fragment orbitals n and σ. Therefore the resonance interaction between the two configurations is roughly proportional to the overlap integral between these fragment orbitals.[51]

Maximization of this overlap requires some bending of the H–X–H angle inward, to flank the lone-pair hybrid. Thus, the

(48) (a) Epiotis, N. D.; Larson, J. R. *Isr. J. Chem.* **1983**, *23*, 53. Epiotis, N. D. *Lect. Notes Chem.* **1983**, *34*, 265–298. (b) See also, ref 10a and 10b, pp 202–203, 209, 313.

(49) The wave function reads $\psi(\mathbf{20}) = N[p\bar{\sigma}^*\sigma - \bar{p}\sigma^*\sigma]$. Note that the p–σ* bond pair is described by a Heitler–London type spin pairing ($\alpha\beta - \beta\alpha$).

(50) The wave function reads $\psi(\mathbf{22}) = N[p\bar{\sigma}^*n\sigma\bar{\sigma} - \bar{p}\sigma^*n\sigma\bar{\sigma}]$.

(51) See, for example, ref 10b, p 315.

deviation from H-X-H linearity is a measure of the weight of the (n → σ*) configuration in the hypercoordinated species. Indeed, as seen in Figure 3, SiH_5 belongs to the D_{3h} symmetry with a linear axial angle. The H-S-H angle in SH_3 is calculated to be 178.0°, whereas the H-P-H angle is 169.9°, and in both cases the bending is toward the hybrid. This confirms the analysis that the (n → σ*) configuration plays a lesser role in SH_3 than in PH_4.

To summarize, the lone pair acts as an electron reservoir that stabilizes the hypercoordinated radicals and affects their geometries and bonding features.

C. Trends in the Hypercoordinated Families. The factors contributing to the stability of the hypercoordinated species are the *weakness* of the X-H bond in the normal-valent species and the *low* ionization potential of the lone pair on H_nX, if such a lone pair exists. The variation of these factors in the periodic table[52] can be presented schematically by **26**. Thus, in each of the

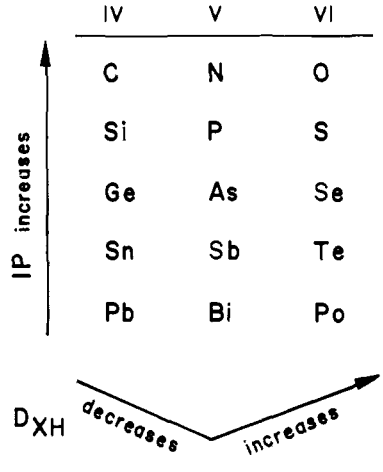

26

families, both IP and *D* decrease down the column, and the corresponding hypercoordinated radicals XH_{n+1} should become increasingly stable and approach or exceed in stability the normal-valent constituents, XH_n + H (see **8**, **9**, and Figure 2). Concomitantly the lowering of the lone-pair ionization potential will induce a greater involvement of the (n → σ*) configuration (**22**) in bonding in the Vth and VIth families.

As we move across a period in the table, **26**, the X-H bond energy first decreases and then increases.[45,46] This effect by itself makes the $X^{(V)}H_4$ species the most stable ones in each period. The lack of a lone pair distinguishes the $X^{(IV)}H_5$ species as the least stable in each period.

As we move down the IVth family (C → Pb) the X-H bond strength, in the normal-valent species XH_4, decreases.[45,46] As mentioned above, the diagram gap *G* is proportional to this bond strength so that ΔE also decreases down the family (C → Pb). In the line of the above discussion, the series XH_5 is expected to exhibit a transition in the direction **8** → **9**. We cannot tell which of the hypercoordinated radicals, if at all, will be a stable species (**9**). However, based on our previous experience with the hypercoordinated trimers, X_3,[13c] we can draw some guidelines. Thus, a very small bond energy (about 20 kcal/mol for X_2, X = alkali atoms) is required to stabilize a hypercoordinated X_3 trimer such as Li_3.[13b,c] On the other hand, bond energies of more than 60 kcal/mol result in hypercoordinated transition states like **8**.[13b,c] Based on this correlation, judgement dictates that CH_5, SiH_5,[53] and perhaps even GeH_5 are expected to be hypercoordinated transition states with decreasing energy. We do not know the Sn-H and Pb-H bond energies, but they may be estimated at 50-60 kcal/mol, a value that suggests that SnH_5 and PbH_5 may

(52) See ref 42b and ref 42a pp 16, 17. Note that in the VIth family we refer to the n lone pair and not the p lone pair.[41]

(53) The result for SiH_5 is now confirmed at the correlated MP2 level: Maitre, P.; Pelissier, M.; Volatron, F., manuscript in preparation.

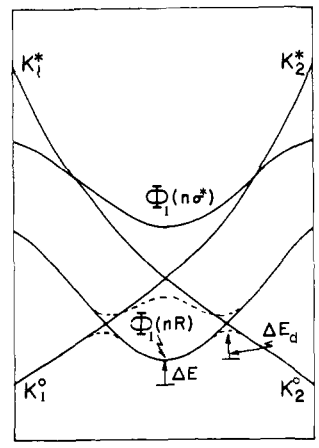

Figure 4. Curve-crossing diagram for cases where the intermediate configuration involve an (n → R) (R ≡ Rydberg) excitation relative to Φ_R and Φ_P.

be at the boundary between **8** and **9**, with PbH_5 tending toward **9**. A possibility for a metastable $X^{(IV)}H_5$ can be envisioned if an intermediate curve of the charge-transfer type (H^-/XH_4^+) becomes low enough to mix into the Lewis curves.

The lone-pair ionization potential of $X^{(VI)}H_2$ is higher than that in $X^{(V)}H_3$.[52] The result is that every hypercoordinated $X^{(V)}H_4$ is expected to be markedly more stable than a hypercoordinated $X^{(VI)}H_3$. Therefore, as we move down the columns of these two families there exist increasing chances to observe stable $X^{(IV)}H_4$ species that are like Figure 2b and $X^{(VI)}H_3$ species that are like Figure 2a; all these are with due consequences on the bonding features and electronic characters of these species, in terms of the involvement of the (n → σ*) configurations.

Valence versus Rydberg Hypercoordinated Radicals

A. First-Row Hypercoordinated Radicals. A similar analysis can be used for the hypercoordinated radicals of first-row atoms. Two major differences arise when going from a second-row atom to the corresponding first-row one. First, the bond energy becomes stronger (see **26**). For example, the average N-H bond energy in NH_3 is 93.4 kcal/mol,[46] whereas that of the P-H bond in PH_3 is only 76.7 kcal/mol.[46] This means that the energy gap *G* in Figure 1 becomes larger. Second, the first-row atoms are more electronegative than the corresponding second-row ones. Therefore the lone pair in XH_n is deeper in energy, which leads to a higher energy (n → σ*) configuration. As a consequence, the mixing of the three configurations Φ_R, Φ_P, and (n → σ*) as in Figures 1 and 2 cannot account for any stability of the first-row hypercoordinated radicals, though such species are observed.[28,29,34]

Together with the above qualifications, the presence of the lone pair on XH_n is imperative for achieving the electronic reorganization that is required to stabilize first-row hypercoordinated species. This is achieved by an intermediate configuration arising from an excitation of an electron from n to a Rydberg orbital, R; an (n → R) configuration.

The corresponding avoided crossing diagram is shown in Figure 4. The anchor point of the (n → R) configuration is schematically represented by **27** with one electron occupying a lone pair and

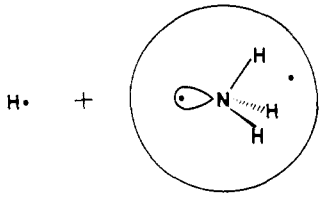

the other, a diffuse Rydberg orbital. The incoming hydrogen atom should attack along the singly occupied lone pair orbital. It therefore leads to tetrahedral and triangular geometries for NH_4 and OH_3, respectively. Quantitative ab initio calculations confirm these results.[30,33,35,36] At this geometry, the Rydberg state (XH_{n+1}) (n → R) possesses a lower energy than the valence species,

(XH_{n+1}), that arises, in Figure 4, from the avoided crossing of the two Lewis configurations, Φ_R and Φ_P. Owing to the diffuseness of the Rydberg orbital, there is only little mixing between the (n → R) curve and the Lewis curves. Therefore, both NH_4 and OH_3 are essentially described in the hypercoordinated region by the (n → R) configuration and may be described as Rydberg hypercoordinated species. Similar conclusions about NH_4 have been derived by Kassab and Evleth[33] using MO theoretical arguments.

The formation energy (ΔE) of NH_4 from its components NH_3 and H has been measured by Porter.[28a] It is customary[33] to relate ΔE to some properties of NH_4, NH_3, and H by using the thermochemical cycle in eq 3a–d.

$$NH_4 \rightarrow NH_4^+ + e^- \qquad IP(NH_4) = 109 \text{ kcal/mol} \quad (3a)$$

$$NH_4^+ \rightarrow NH_3 + H^+ \qquad PA(NH_3) = 202 \text{ kcal/mol} \quad (3b)$$

$$H^+ + e^- \rightarrow H^\bullet \qquad -IP(H) = -314 \text{ kcal/mol} \quad (3c)$$

$$NH_4 \rightarrow NH_3 + H^\bullet \qquad IP(NH_4) + PA(NH_3) - IP(H) = -3 \text{ kcal/mol} \quad (3d)$$

The second step involves the proton affinity of NH_3,[54] and the third step corresponds to the negative value of the ionization potential of hydrogen. The ionization potential of NH_4, corresponding to the first step, has been estimated by Porter to be 109 kcal/mol, so as to account for the measured value of ΔE. This value represents the attraction between NH_4^+ and a far away Rydberg electron, **28**.

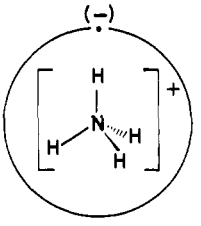

28

We can then estimate ΔE for other species using eq 4. In the

$$\Delta E(XH_n + H^\bullet \rightarrow XH_{n+1}) = IP(H) - IP(XH_{n+1}) - PA(XH_n) \quad (4)$$

right-hand side of this equation the only variable is the third term, $PA(XH_n)$, if we assume the second term to be insensitive to the nature of the central $(XH_{n+1})^+$ core. Thus the larger the $PA(XH_n)$, the more stable the Rydberg-hypercoordinated state. Using $PA(H_2O)$,[42a] we obtain $\Delta E = +35$ kcal/mol, which compares favorably with the best computational results, ranging between +26 and +36 kcal/mol.[35,36]

The ΔE values for NH_4 and OH_3 suggest also a higher dissociation barrier for NH_4 to the normal-valent constituents (ΔE_d in Figure 4). This last conclusion is supported by the theoretical calculations, the dissociation barriers of NH_4 being calculated to be 15.0,[30] 15.3,[31] 14.8,[32] and 12.0[33] kcal/mol, whereas those of OH_3 are 6.6[35] and 3.4[36] kcal/mol.

B. Second-Row Hypercoordinated Radicals Are Not Rydberg Species. Why? Equation 4 provides a rationale for the quite puzzling fact that despite the possible stability of Rydberg hypercoordinated species, these are not observed for second-row species, PH_4, SH_3, and so on. Using cycle 3 and experimental proton affinities,[42a] the ΔE values for possible Rydberg PH_4 and SH_3 are +25 and +41 kcal/mol, respectively. Both values are substantially larger than the calculated ΔE's in Table I for the valence species. We may then conclude that Rydberg hypercoordinated species will be of higher energies than the valence species when the hypercoordinated atom is *not* a first-row atom.

We actually computed the energy of the Rydberg state of PH_4 by first optimizing the geometry of PH_4^+ (P–H = 1.380 Å) in tetrahedral geometry and then optimizing the exponent ζ of the phosphor Rydberg orbital ($\zeta = 0.020$) for the neutral compound in the same geometry. We found the Rydberg state to be 26 kcal/mol above the ground state, thus confirming the above analysis.

The crucial role of a lone pair in generating Rydberg hypercoordination is projected by the fact that contrary to NH_4 and OH_3, CH_5 is a valence species that is a transition state for hydrogen exchange with $\Delta E \cong +61$ kcal/mol.[37,38,56,57]

In summation, Rydberg hypercoordinated radicals will possess significant stability if the proton affinity of the corresponding XH_n^+ is larger than 200 kcal/mol. This condition restricts Rydberg hypercoordination to first-row radicals whose normal-valent XH_n possess a lone pair with a low energy.

Conclusions

Hypercoordinated XH_{n+1} radicals fall into two broad classes of valence species: those that can be described by avoided crossings of their two Lewis curves (Figure 1 and **8**, **9**), e.g., SiH_5 and those that require at least one additional curve—termed the intermediate curve, e.g., PH_4. The intermediate curve may possess an (n → σ*) character which mixes into the Lewis curves and thereby endows a valence hypercoordinated species with additional stability and a new electronic character (Figure 2 and **18**, **19**). On the other hand, the intermediate curve may be of Rydberg character (n → R excitation) and provide an energy well to house a Rydberg XH_{n+1} radical (Figure 4).

The model predicts that the hypercoordination capability of an atom X depends on the weakness of the X–H bond, in the normal-valent XH_n, and on the presence of a lone pair (on H_nX) with a low ionization potential. The first factor determines the stability of XH_{n+1} as a result of avoided crossing of the two Lewis curves, and this stability increases as the X–H bond (of XH_n) becomes weaker and weaker (**8** → **9**). The second factor provides a low-lying (n → σ*) or a (n → R) curve that crosses the two Lewis curves and may provide metastable XH_{n+1} radicals even when the X–H bond is strong (Figure 2a). The following general and specific conclusions may be noted:

Due to the lowering of both bond strength and lone-pair ionization potential, the stability of the hypercoordinated species is predicted to increase as we go down each column in the periodic table (**26**). Due to the same effects, it is predicted that the stability of XH_{n+1} should peak when X belongs to the Vth family (e.g., PH_4) in each period.

PH_4 and SH_3 are possible candidates for stability since the (n → σ*) configuration stabilizes the hypercoordinated species. Our qualitative analysis suggests that PH_4 is more stable than SH_3 on both accounts of bond strength and lone-pair ionization potential, both being lower for PH_4. In agreement with the above tendencies, PH_4 has been isolated and is actually a stable or a metastable radical, whereas SH_3 has been demonstrated to be a transition state or a metastable species with a tiny barrier for decomposition to $SH_2 + H$.[25]

First-row XH_{n+1} radicals may occur as stable or metastable species due to the involvement of the (n → R) Rydberg curve. A high proton affinity of XH_n is required (PA larger than 200 kcal/mol) to stabilize a first-row XH_{n+1} Rydberg radical. NH_4 and OH_3 are such species, with the former being the most stable one. A barrier to dissociation to $XH_n + H$ arises due to avoided crossing of Rydberg and valence configurations.

The lack of a lone pair and the strong Si–H and C–H bonds prohibit any pronounced stability for SiH_5 and CH_5 which should most likely be transition states in the hydrogen-exchange reactions, like Figure 1 or **9**. CH_5 is actually a transition state as previously demonstrated by means of ab initio calculations.[37,38] Our preliminary calculations[53] on the D_{3h} SiH_5 system indicate that this molecule does not display any Rydberg character in its ground state, which rules out any intervention of a Rydberg excited configuration (σ → R). Since no intermediate configuration may intervene and owing to the Si–H bond strength, SiH_5 seems more

(54) Williams, B. W.; Porter, R. F. *J. Chem. Phys.* **1980**, *73*, 5598.
(55) Page 18 of ref 42a.
(56) Schwarz, W. H. E. *Chem. Phys.* **1975**, *11*, 217.
(57) Raynor, S.; Herschbach, D. R. *J. Phys. Chem.* **1982**, *86*, 3592.

likely to be a transition state rather than a stable structure. This prediction is at variance with the conclusions drawn by Nakamura et al.[22]

The curve-crossing model thus unifies the hypercoordination problem with the delocalization[13] and reactivity problems.[10-13] On the basis of elementary thermochemistry, it is possible to pattern the trends in the stability of hypercoordinated, delocalized, and transition-state species relative to their normal-valent constituents. Extension to other hypercoordinated radicals is in progress.

Acknowledgment. We are grateful to Dr. J. Roncin for helpful discussions and to Dr. E. Evleth for communicating his results to us prior to publication. S.S.S. thanks the Université de Paris-Sud for a Visiting Professorship, during which time this paper was shaped. We thank the scientific committee of the CCVR for a grant (ATP 3872) on the Cray-1S computer (Palaiseau).

Theoretical Study of the Electronic Structures and Absorption Spectra of $Pt(CN)_4^{2-}$ and $Tl_2Pt(CN)_4$ Based on Density Functional Theory Including Relativistic Effects

Tom Ziegler,*,† Jeffrey K. Nagle,*,‡ Jaap G. Snijders,§ and Evert J. Baerends§

Contribution from the Department of Chemistry, University of Calgary, Calgary, Alberta, Canada T2N 1N4, Department of Chemistry, Bowdoin College, Brunswick, Maine 04011, and Department of Theoretical Chemistry, Free University, De Boelelaan 1083, 1081 HV Amsterdam, The Netherlands. *Received August 22, 1988*

Abstract: Density functional calculations on $Pt(CN)_4^{2-}$ (**1**) and the recently reported $Tl_2Pt(CN)_4$ (**2**) have been carried out in both the nonrelativistic and quasi-relativistic limits. This has led to a new and detailed understanding of the electronic structure of **1**. Electronic transition energies for **1** have been calculated from state function energy differences to help clarify many of the spectroscopic properties of this ion. This is the first time such calculations have been performed using density functional theory. The interaction between **1** and Tl^+ ions in **2** is shown to be largely ionic in nature but with a substantial covalent component (189 kJ mol^{-1}). It is suggested that the Tl^+ ions in **2** provide a spectroscopic probe that could enable a rigorous comparison to be made between electronic structure calculations and polarized single-crystal absorption and emission spectra.

The bonding and spectroscopy of $Pt(CN)_4^{2-}$ (**1**) continue to attract attention.[1] As an isolated ion it serves as a model for understanding the bonding and spectroscopic properties of d^8 square-planar compounds possessing strong field ligands. Perhaps even greater interest centers on the ability of **1** to form columnar structures in the solid state with adjacent Pt atoms separated by 310-370 pm.[2] Such stacking results in the appearance of a low-energy absorption band often accompanied by a corresponding visible luminescence.[1]

Despite many attempts over the years, both experimental and theoretical, some issues regarding the bonding and spectroscopic properties of **1** remain unresolved.[1] Perhaps the greatest uncertainty concerns the relative energy ordering of the Pt 5d orbitals and its effect on the spectroscopic properties of the ion. This ordering has important implications also for establishing the mechanism by which the ions stack to form columnar structures.

Although more than 20 different columnar compounds containing **1** and various metal ions are known,[2] the recently reported structure of $Tl_2Pt(CN)_4$ (**2**) reveals it to be unique in that it is not columnar but consists of discreet octahedral molecules with Pt-Tl bonds.[3] As such it serves as perhaps the simplest example of a growing class of structurally characterized compounds found to possess relatively short internuclear distances between d-block elements like Ir, Pt, and Au and p-block elements like Tl and Pb.[4] Evidence has been obtained for the presence of covalent metal-metal interactions in these[4] and related but structurally uncharacterized compounds.[5] The recent report of a strongly luminescent exciplex formed between $Pt_2(P_2O_5H_2)_4^{4-}$ and Tl^+ in aqueous solution is also of interest in this context.[6] It is therefore of some importance to determine the nature of the bonding in **2** to see if any useful generalizations can be made about the bonding in this group of compounds.

One of the best ways to understand the bonding and spectroscopy in **1** and **2** is to do reliable electronic structure calculations. Reported here are the results of density functional calculations on **1** and **2**. Relativistic effects have been taken into account due to the presence of the heavy Pt and Tl atoms. Detailed spectroscopic assignments based on the inclusion of spin-orbit coupling are possible using this approach and enable a comparison with the well-studied spectrum of **1** to be made. This is the first relativistic density functional calculation on the electronic spectrum

† University of Calgary.
‡ Bowdoin College.
§ Free University.

(1) For recent reviews and pertinent references, see: Gliemann, G.; Yersin, H. *Struct. Bonding* **1985**, *62*, 89-153. Hoffmann, R. *Angew. Chem., Int. Ed. Engl.* **1987**, *26*, 846-878.
(2) Williams, J. M. *Adv. Inorg. Chem. Radiochem.* **1983**, *26*, 235-268.
(3) Nagle, J. K.; Balch, A. L.; Olmstead, M. M. *J. Am. Chem. Soc.* **1988**, *110*, 319-321.
(4) (a) $Ir_2M(CO)_2Cl_2\{\mu\text{-}[(C_6H_5)_2PCH_2]_2As(C_6H_5)\}_2^+$ (M = Tl, Pb): Balch, A. L.; Nagle, J. K.; Olmstead, M. M.; Reedy, P. E., Jr. *J. Am. Chem. soc.* **1987**, *109*, 4123-4124. (b) $Tl[Au(CN)_2]$: Blom, N.; Ludi, A.; Bürgi, H.-B.; Tichy, K. *Acta Crysallogr., Sect. C: Cryst. Struct. Commun.* **1984**, *C40*, 1767-1769. (c) $Pt[P(C_6H_5)_3]_2[Pb(C_6H_5)_3]_2$: Crocinai, B.; Nicolini, M.; Clemente, D. A.; Bandoli, G. *J. Organomet. Chem.* **1973**, *49*, 249-256. (d) $AuTl[(C_6H_5)_2P(CH_2)S]_2$: Wang, S.; Fackler, J. P., Jr.; King, C.; Wang, J. C. *J. Am. Chem. Soc.* **1988**, *110*, 3308-3310. (e) $Au_2Pb[(C_6H_5)_2P(CH_2)S]_4$: Wang, S.; Garzon, G.; Wang, J. C.; Fackler, J. P., Jr., unpublished results. (f) $TlPt_3(CO)_3[P(C_6H_{11})_3]_3^+$: Ezomo, O. J.; Mingos, D. M. P.; Williams, I. D. *J. Chem. Soc., Chem. Commun.* **1987**, 924-925.
(5) (a) $PtL_2[Pb(C_6H_5)_3]_2$ [L = $P(C_2H_5)_3$, $As(C_2H_5)_3$]: Deganello, G.; Carturan, G.; Belluco, U. *J. Chem. Soc. A* **1968**, 2873-2878. (b) $Pt[P(C_6H_5)_3]_2(Br)_2(C_6H_5)[Tl(C_6F_5)Br]$: Nyholm, R. S. *Q. Rev.* **1970**, *24*, 1-19. (c) $Ir(CO)(O_2CR)L_2X[Tl(O_2CR)_2]$ (R = CH_3, C_2H_5, $CH(CH_3)_2$, CF_3, L = $P(C_6H_5)_3$, $P(CH_3)_2C_6H_5$, $As(C_6H_5)_3$; X = Cl, O_2CR): Van Vliet, P. I.; Vrieze, K. *J. Organomet. Chem.* **1977**, *139*, 337-347. (d) $\{Ir(bta)_2[P(C_2H_5)_3Tl\}\cdot C_6H_6$ (bta = benzotriazenido): Brown, L. D.; Ibers, J. A.; Siedle, A. R. *Inorg. Chem.* **1978**, *17*, 3026-3030.
(6) Nagle, J. K.; Brennan, B. A. *J. Am. Chem. Soc.* **1988**, *110*, 5931-5932.

0002-7863/89/1511-5631$01.50/0